


 Cite this: *RSC Adv.*, 2020, **10**, 26326

Long-range ferromagnetic order in perovskite manganite $\text{La}_{0.67}\text{Ba}_{0.25}\text{Ca}_{0.08}\text{Mn}_{(1-x)}\text{Ti}_x\text{O}_3$ ($x = 0.00, 0.05$ and 0.10)

 Marwa Bourguiba,^{ab} Mohamed Amara Gdaiem,^{id *c} Moez Chafra^a and E. K. Hlil^d

In this study, we report the effects of Ti on the critical behavior of $\text{La}_{0.67}\text{Ba}_{0.25}\text{Ca}_{0.08}\text{MnO}_3$ samples prepared by the flux method. Moreover, the critical exponents β , γ and δ are estimated through numerous techniques such as the modified Arrott plot, the Kouvel–Fisher method and critical isotherm analysis of the magnetic measurements on record near the Curie temperature. Compared to standard models, the estimated critical exponents are close to the theoretical values of the mean-field model for these samples. In order to estimate the spontaneous magnetization at a given temperature, we used a process based on the analysis, in the mean-field theory, of the magnetic entropy change ($-\Delta S_M$) vs. magnetization (M). An excellent agreement was found between the spontaneous magnetization determined from $-\Delta S_M$ vs. M^2 and the classical extrapolation from the Arrott curves ($\mu_0 H/M$ vs. M^2), thus confirming that $-\Delta S_M$ is a valid approach to estimate the spontaneous magnetization in this system. The accuracy of the critical exponent values was confirmed with the scaling hypothesis. The magnetization curves fall onto one of two sides, below and above T_C .

 Received 1st May 2020
 Accepted 3rd June 2020

DOI: 10.1039/d0ra03949g

rsc.li/rsc-advances

1. Introduction

Hole-doped manganite perovskites $\text{La}_{1-x}\text{A}_x\text{MnO}_3$ ($\text{A} = \text{Ca}, \text{Sr}$, and Ba) have attracted extensive attention. This is owing to their peculiar magnetic properties and their potential technological applications and in particular the discovery of colossal magnetoresistance (CMR) in recent years.^{1–5} For $x = 0$, the ground state compound of LaMnO_3 is an insulating A-type canted antiferromagnetic (AFM) state with $T_N = 140$ K.⁶ With Sr-doped lanthanum manganites, the magnetic properties highly depend on the content of x .⁷ The ferromagnetic (FM) materials generated by doped holes are attributed to the double exchange (DE) effect, in which eg electrons transfer between adjacent Mn^{3+} and Mn^{4+} ions, and to the Jahn–Teller effect.⁸ For $x = 0.5$, the compound with a tetragonal phase is characterized by an FM curie temperature (T_C) $T_C = 310$ K and undergoes a transition to the A-type AFM order at $T_N = 220$ K.⁹ To further understand the FM-paramagnetic (PM) transition in the bulk material, M. Hazzez *et al.* calculated the critical exponents of $\text{La}_{0.5}\text{Sr}_{0.5}\text{MnO}_3$ synthesized by a solid state reaction and showed that the transition is of a second order, corresponding to the mean-field model with critical

exponents $\beta = 0.507$ and $\gamma = 1.107$, which is dominated by long-range interactions around T_C .¹⁰ Recently, the lanthanum strontium manganites have been extensively studied on a nanoscale due to the potential applications in magnetic refrigeration, biomedicine and biological research.^{11–13} Numerous attempts have been made to investigate the magnetic nanoparticles for their interesting size effects and surface magnetism.^{14–16} As the particle size decreases, the surface and interface become more important due to the increased surface atoms/bulk atom ratio. The magnetic properties of nanomaterials are strongly influenced by the surface spins and may differ significantly from the bulk material properties. Therefore, it is very important to gain an understanding of the magnetic transition mechanism by investigating the critical behaviors of nano-sized compounds. In the present study, we study the effect of titanium on the critical behavior around the FM–PM phase transition for $\text{La}_{0.67}\text{Ba}_{0.25}\text{Ca}_{0.08}\text{MnO}_3$ samples. Moreover, the critical exponents β , γ and δ are estimated through numerous techniques such as the modified Arrott plot (MAP), Kouvel–Fisher (KF) method and critical isotherm (CI) analysis of the magnetic measurements near T_C .

2. Experimental details

In this study, our samples were prepared by the flux method. La_2O_3 , BaCO_3 , CaCO_3 , MnO_2 and TiO_2 precursors, with high purity, were used. The mixture was ground in an agate mortar for 2 h with an appropriate quantity of KCl . Then, the powder was heated in an alumina crucible at 800 °C for 24 h. Further, it was washed with hot distilled water to remove the KCl salts. The

^aLaboratoire de recherche en Mécanique Appliquée et systèmes (LASMAP-EPT), Ecole Polytechnique de Tunisie, Université de Carthage, La Marsa, Tunisia

^bFaculté des sciences de Tunis, Université de Tunis el Manar, Tunis 2092, Tunisia

^cLaboratoire de la Matière Condensée et des Nanosciences, Département de Physique, Faculté des Sciences de Monastir, 5019, Tunisia. E-mail: gdaiem_mohamed@hotmail.fr; Tel: +21629523640

^dInstitut Néel, CNRS et Université Joseph Fourier, BP 166, 38042 Grenoble, France



residue was dried at 100 °C in air. After being ground well, the powders were pressed into circular pellets ($e = 1$ mm and $d = 10$ mm) at 105 Pa. The pellets were sintered in the air at 1000 °C for 24 h.

Magnetization isotherms were measured in the range of 0–5 T and with a temperature interval of 3 K in the vicinity of T_C . These isotherms are corrected by a demagnetization factor D that was determined by a standard procedure from low-field dc magnetization measurement at low temperatures ($\mu_0 H = \mu_0 H_{app} - DM$).

3. Scaling analysis

In order to clarify the nature of the FM–PM phase transition, deeper insight into the magnetic phase transition should be obtained by analyzing the critical region around T_C . In general, the critical phenomena cannot define the first-order transition for because the magnetic field can affect the transition¹⁷ and create a discontinuity of the order parameter in the vicinity of

the critical temperature. Based on the scaling hypothesis, the critical behavior of our samples, around T_C , was studied using Arrott plots and the critical exponents. β is associated with M_S just below T_C , γ is related to the critical magnetization isotherm at T_C , and δ is related to the initial magnetic susceptibility just above T_C .^{18,19} As is known, four models can usually describe the magnetic interactions in manganites: the mean-field ($\beta = 0.5$, $\gamma = 1.0$ and $\delta = 3.0$), tri-critical mean-field ($\beta = 0.25$, $\gamma = 1.0$ and $\delta = 5.0$), three-dimensional (3D) Heisenberg ($\beta = 0.365$, $\gamma = 1.336$ and $\delta = 4.8$) and 3D-Ising ($\beta = 0.325$, $\gamma = 1.24$ and $\delta = 4.82$) models. This method was based on the equation of state:

$$\left[\frac{H}{M} \right]^{1/\gamma} = \frac{a[T - T_C]}{T} + bM^{2/\beta} \quad (1)$$

The exponent's equations from M measurements are given below:

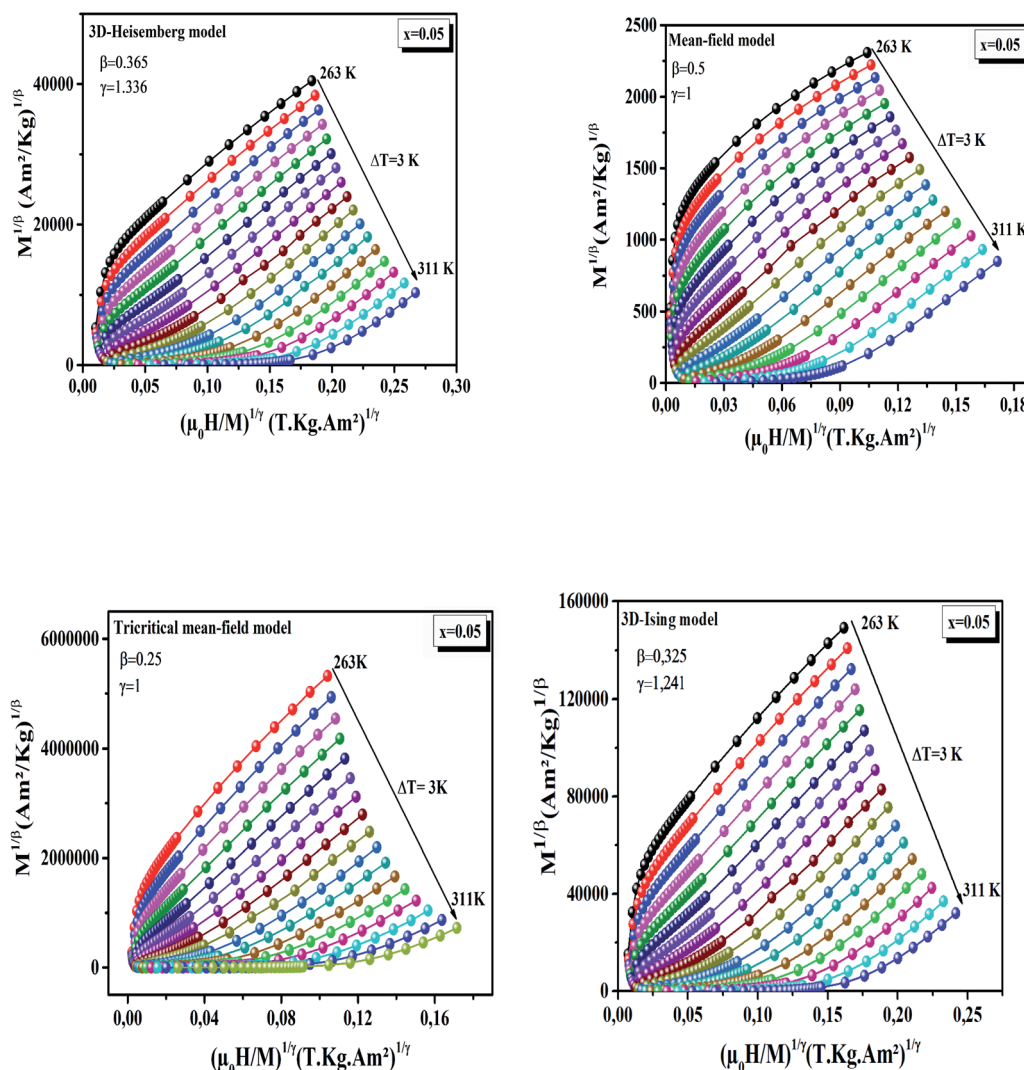
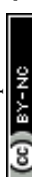


Fig. 1 MAP for $x = 0.05$, an example: Mean-Field model ($\beta = 0.25$, $\gamma = 1$), tri-critical Mean-Field model ($\beta = 0.25$, $\gamma = 1$), 3D-Heisenberg model ($\beta = 0.365$, $\gamma = 1.336$) and 3D-Ising model ($\beta = 0.325$, $\gamma = 1.24$).



$$M_S(T) = m_0(-\varepsilon)^\beta; T < T_C, \varepsilon < 0 \quad (2)$$

$$\chi_0^{-1} = \left(\frac{h_0}{m_0}\right) \varepsilon^\gamma; T > T_C, \varepsilon > 0 \quad (3)$$

$$M(\mu_0 H) = D(\mu_0 H)^{1/\delta}; T = T_C, \varepsilon = 0 \quad (4)$$

Where $\varepsilon = (T - T_C)/T_C$ and M_0 , (h_0/M_0) and D are the critical amplitudes.

Furthermore, in the critical region, M and the internal field should obey the universal scaling behavior, which can be written as:

$$M(\mu_0 H, \varepsilon) = |\varepsilon|^\beta f_\pm M \left(\frac{\mu_0 H}{|\varepsilon|^{\beta+\gamma}} \right) \quad (5)$$

where f_+ for $T > T_C$ and f_- for $T < T_C$. Eqn (5) implies that $M/|\varepsilon|^\beta$ vs. $H/|\varepsilon|^{\beta+\gamma}$ yields two universal curves for a true scaling relation and good values of critical exponents: one for temperatures below T_C and the other for temperatures above T_C .

4. Results and discussion

Using the experimental M data obtained for all of the studied compounds, we determined MAP in order to better understand the nature of the transition around T_C . These curves are obtained from the following equation:²⁰

$$\left(\frac{\mu_0 H}{M} \right)^{\frac{1}{\gamma}} = a \frac{(T - T_C)}{T_C} + b M^{\frac{1}{\beta}} \quad (6)$$

Here, 'a' and 'b' are constants.

Fig. 1 shows $M^{1/\beta}$ vs. $(H/M)^{1/\gamma}$ based on the Arrott–Noakes equation of state eqn (6) at different temperatures for the $x = 0.05$ sample as an example, deduced by using trial critical exponents from several models: mean-field, 3D-Heisenberg, 3D-Ising and tri-critical mean-field. For this analysis, only the high-field linear region is used because at low magnetic fields the magnetic multi-domains are not totally aligned and the MAP deviates from linearity. It is evident in Fig. 1 that all of the models yield quasi-straight and nearly parallel lines in the high field region, making it difficult to decide which model is best to determine the critical exponent.

Thus, to confirm the best model to fit our experimental data, we calculated the so-called relative slope (RS) defined at the critical point as:

$$RS = S(T)/S(T_C) \quad (7)$$

where $S(T)$ is the slope of $M^{1/\beta}$ versus $\mu_0(H/M)^{1/\gamma}$ and $S(T_C)$ is the slope for the curve recorded at $T = T_C$. The most satisfactory model should be the one with the closest RS to 1 (unity).²¹ According to this criterion, and as shown in Fig. 2, mean-field is the most suitable model for all our samples.²² Based on the chosen model, $M_S(T,0)$ and the inverse magnetic susceptibility

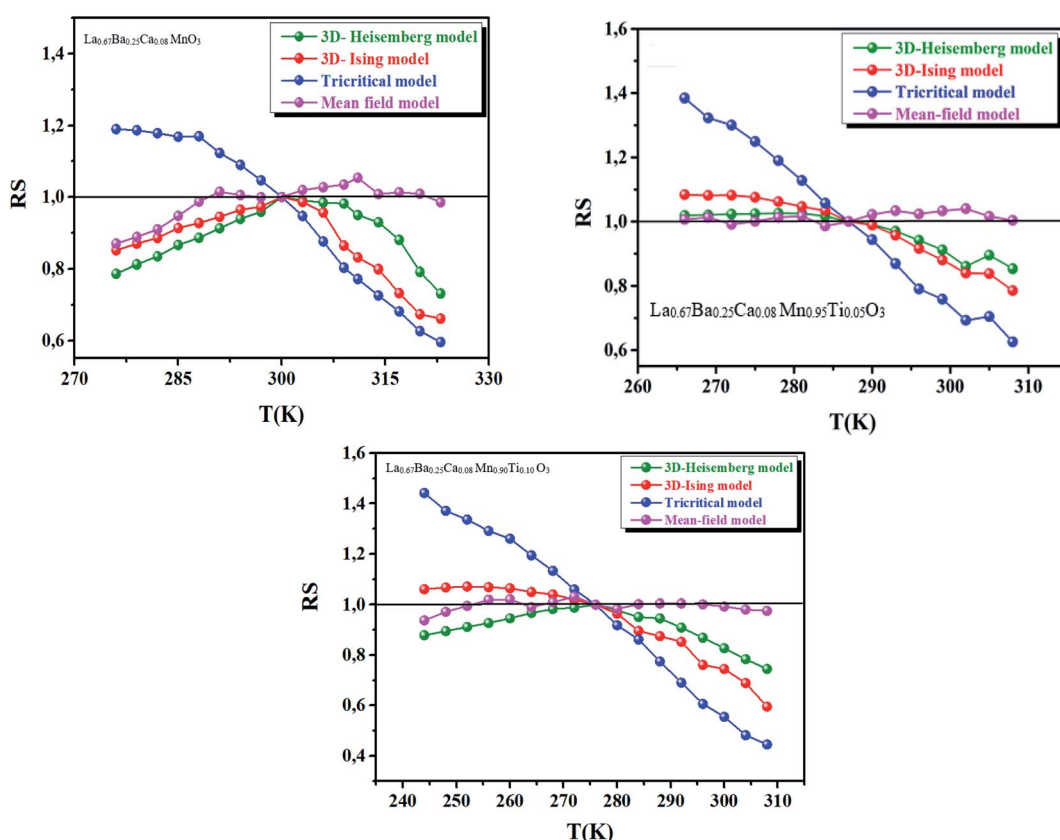


Fig. 2 RS of our samples as a function of temperature defined as $RS = S(T)/S(T_C)$ using several methods.



Table 1 Comparison of critical exponents for our sample from various models: MAP, KF and CI

Samples		T_C (K)	β	γ	δ	Ref.
$x = 0.00$	MAP	301	0.48	1.06	—	This work
	KF	304.15(5)	0.47(5)	1.13(3)	—	
	CI(exp)	300	—	—	3.31(1)	
	CI(cal)	—	—	—	3.37(8)	
$x = 0.05$	MAP	291.17(8)	0.45(4)	1.02(0)	—	This work
	KF	291.69(3)	0.46(1)	1.03(0)	—	
	CI(exp)	287	—	—	3.25(2)	
	CI(cal)	—	—	—	3.23(4)	
$x = 0.10$	MAP	280.08(4)	0.48(8)	1.09(8)	—	This work
	KF	279.99(2)	0.478(8)	1.12(5)	—	
	CI(exp)	277	—	—	3.22(5)	
	CI(cal)	—	—	—	3.33(9)	
Mean field model	—	0.5	1	3	30	
3D Heisenberg model	—	0.365	1.336	4.80	30	
3D Ising model	—	0.325	1.241	4.82	30	
Tricritical model	—	0.25	1	5	31	
$\text{La}_{0.67}\text{Ca}_{0.33}\text{Mn}_{0.95}\text{Fe}_{0.05}\text{O}_3$	162	0.552	1.024	2.801	32	
$\text{La}_{0.6}\text{Ca}_{0.4}\text{MnO}_3$	267.88	0.248	0.995	4.896	33	
$\text{La}_{0.67}\text{Ba}_{0.33}\text{Mn}_{0.98}\text{Ti}_{0.02}\text{O}_3$	310	0.551 ± 0.008	1.020 ± 0.024	2.851	34	
$\text{La}_{0.7}\text{Ca}_{0.3}\text{Mn}_{0.95}\text{Ti}_{0.05}\text{O}_3$	136	0.601 ± 0.02	1.171 ± 0.01	2.95 ± 0.01	35	
$\text{La}_{0.67}\text{Ba}_{0.33}\text{MnO}_3$	306	0.356 ± 0.004	1.120 ± 0.003	4.15 ± 0.05	36	

$[\chi_0^{-1}(T)]$ were obtained from the intersections of the linear extrapolation line in the high field region of $(M_S)^{1/\beta}$ with the $(H/M)^{1/\gamma}$ axis.

Fig. 3 shows the power law fittings of the temperature dependence of $M_S(T,0)$ and $\chi_0^{-1}(T,0)$. New values of β , γ and T_C were obtained by fitting the plots of $M_S(T,0)$ and $\chi_0^{-1}(T,0)$ with eqn (1) and (2), respectively. The results of the fits for our

samples are also presented in the same figure and listed in Table 1. Subsequently, convergence was reached by the reasonable values of the critical parameters. These values are very close to the critical exponents of the mean-field model, as displayed in Table 1.

The third parameter ‘ δ ’ was determined precisely from $M(T_C, \mu_0 H)$ at $T = T_C$ using eqn (4). We plotted these isotherms

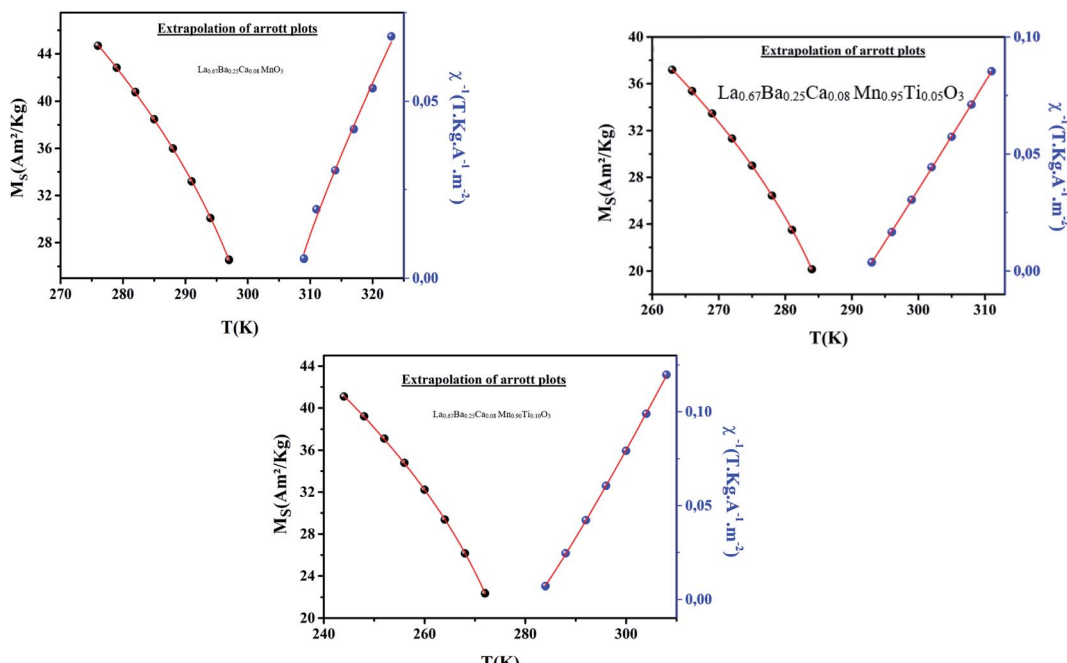


Fig. 3 Temperature dependence of the spontaneous magnetization $M_S(T,0)$ (left) and the inverse initial susceptibility $\chi_0^{-1}(T)$ (right), with the fitting curves based on the power laws.



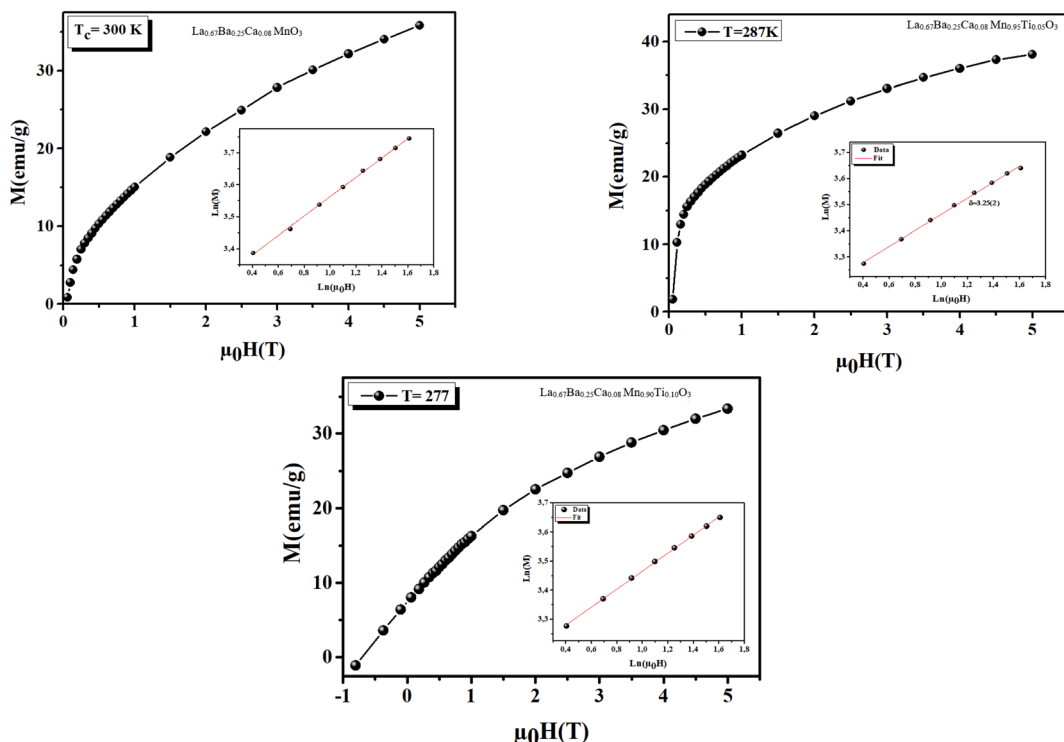


Fig. 4 Isothermal $M(T_C, \mu_0 H)$ plot for our samples at T_C . The insets show the same plot in log–log scale for each sample, and the solid line is the linear fit following eqn (4) for the determination of the critical exponent δ .

together with the log–log plot of M versus $\mu_0 H$ (inset of Fig. 4). As seen in the high-field region, the log–log plots are straight lines with the slope $1/\delta$. The critical exponents from this static scaling analysis are related to the Widom scaling relation $\delta = 1 + \gamma/\beta$.²³ Using this relation and the estimated values of γ and β (obtained above) from the mean-field method, we obtained results close to the values obtained from the critical isotherms. The

estimated values of δ for all of the samples are given in Table 1. These values are consistent with the prediction of the mean-field theory ($\beta = 0.5$, $\gamma = 1$, and $\delta = 3$).²⁴

Another method to find the critical exponents and T_C more accurately is the KF method, which is expressed in the following equations:²⁵

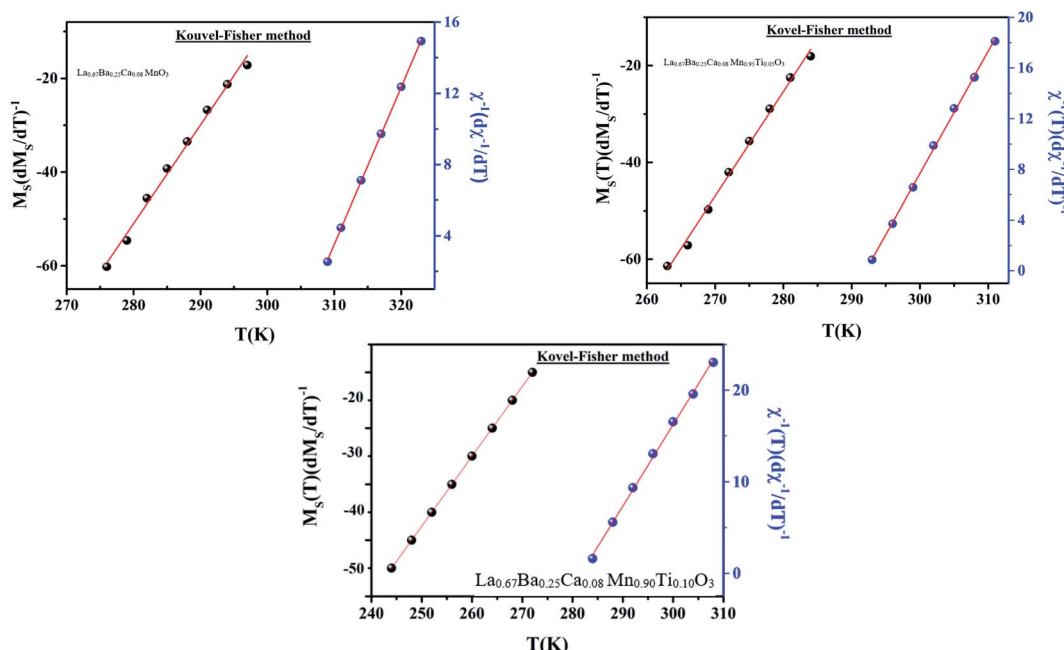


Fig. 5 KF plots for the spontaneous magnetization (left) and the inverse initial susceptibility $\chi_0^{-1}(T)$ (right) for our samples.

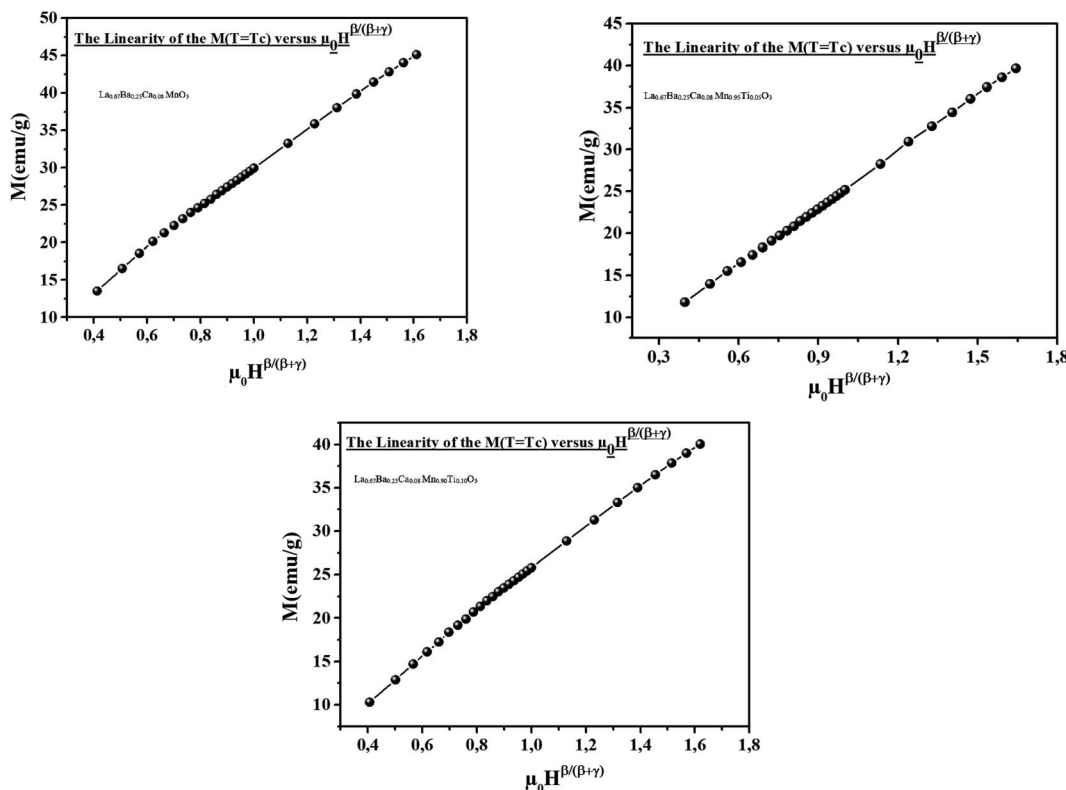


Fig. 6 $M(T_C)$ versus $(\mu_0 H)^{\beta/(\beta+\gamma)}$ plots for our samples.

$$M_S(T) \left[\frac{dM_S(T)}{d(T)} \right]^{-1} = \frac{T - T_C}{\beta} \quad (8)$$

$$\chi_0^{-1}(T) \left[\frac{d\chi_0^{-1}(T)}{d(T)} \right]^{-1} = \frac{T - T_C}{\gamma} \quad (9)$$

The temperatures of $M_S(T) \left[\frac{dM_S(T)}{d(T)} \right]^{-1}$ and $\chi_0^{-1}(T) \left[\frac{d\chi_0^{-1}(T)}{d(T)} \right]^{-1}$ are shown in Fig. 5. The fit of these curves by eqn (8) and (9) leads to the determination of the critical exponents γ , β and T_C . The obtained values for these exponents are summarized in Table 1. Noticeably, these values are also in a good agreement with those obtained from MAP.

The Widom relationship was tested by plotting $M(T = T_C)$ versus $(\mu_0 H)^{\beta/(\beta+\gamma)}$ and checking the linearity of the curve, as shown in Fig. 6.

The reliability of the critical exponents determined experimentally can be verified using a more rigorous method¹⁸ based on the prediction of the scaling hypothesis in the critical region, through which the applied magnetic field $\mu_0 H$ and M can be related in the vicinity of T_C by eqn (5). Fig. 7 shows that for each compound, two universal curves are obtained: the first one for temperature values below T_C and the second one for temperature values above T_C . Hence, the critical exponents and the critical temperature T_C agreed well with the scaling hypothesis.

In addition, in homogeneous magnets and based on the renormalization group analysis of systems performed by Fisher *et al.*, the universality class of the magnetic phase transition depends strongly on the range of the exchange interaction, as described by the following equation:²⁶

$$J(r) = 1/r^{d+\sigma} \quad (10)$$

where r is the distance between the interaction spins, d is the dimension of the system and $\sigma > 0$ is the range of the interaction.

For a three-dimensional material ($d = 3$), the relationship is $J(r) = 1/r^{3+\sigma}$ with $3/2 \leq \sigma \leq 2$. In general, if $J(r)$ decreases faster than r^{-5} (r greater than 2), the Heisenberg exponents ($\beta = 0.365$, $\gamma = 1.336$ and $\delta = 4.8$) are valid for a 3D-isotropic ferromagnet. However the MF-theory ($\beta = 0.5$, $\gamma = 1.0$ and $\delta = 3.0$) exponents are valid for $\sigma < 1/2$ if $J(r)$ decreases with the “long-range” distance slower than $r^{-4.5}$. In the intermediate range, if $1/2 < \sigma < 2$, the exponents belong to other universality classes (such as the TMF theory and the 3D-Ising model). In the case of our samples, the values of the critical exponents are in agreement with the mean-field model. Consequently, $(d + \sigma)$ will be smaller than 4.5, and the exchange interaction $J(r)$ drops slower than $r^{-4.5}$ for our samples.

The following section shows an attempt to do theoretical modeling of M_S based on the mean-field analysis of $-\Delta S_M$.²⁷ A general result issued from the mean-field theory reveals the dependence of $-\Delta S_M$ on the relative M is described as:^{28,29}

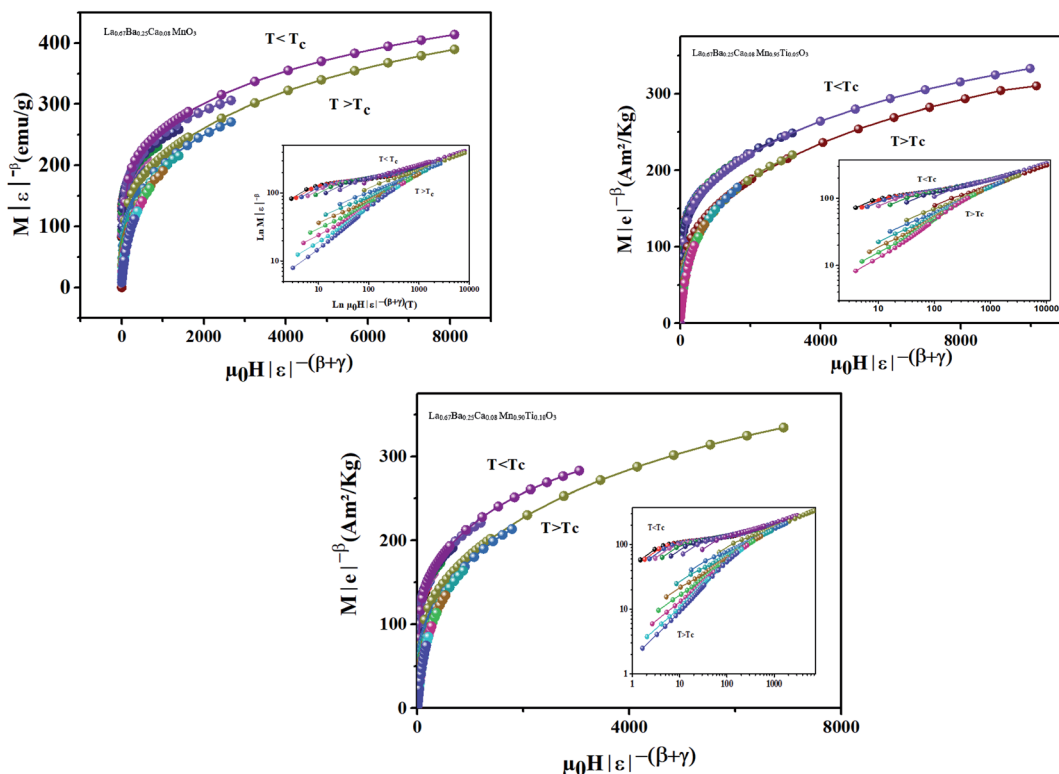


Fig. 7 Scaling plots $M|\varepsilon|^{-\beta}$ vs. $\mu_0 H|\varepsilon|^{-(\beta+\gamma)}$, indicating two universal curves below and above T_C for our samples. Inset shows the same plots on a log-log scale.

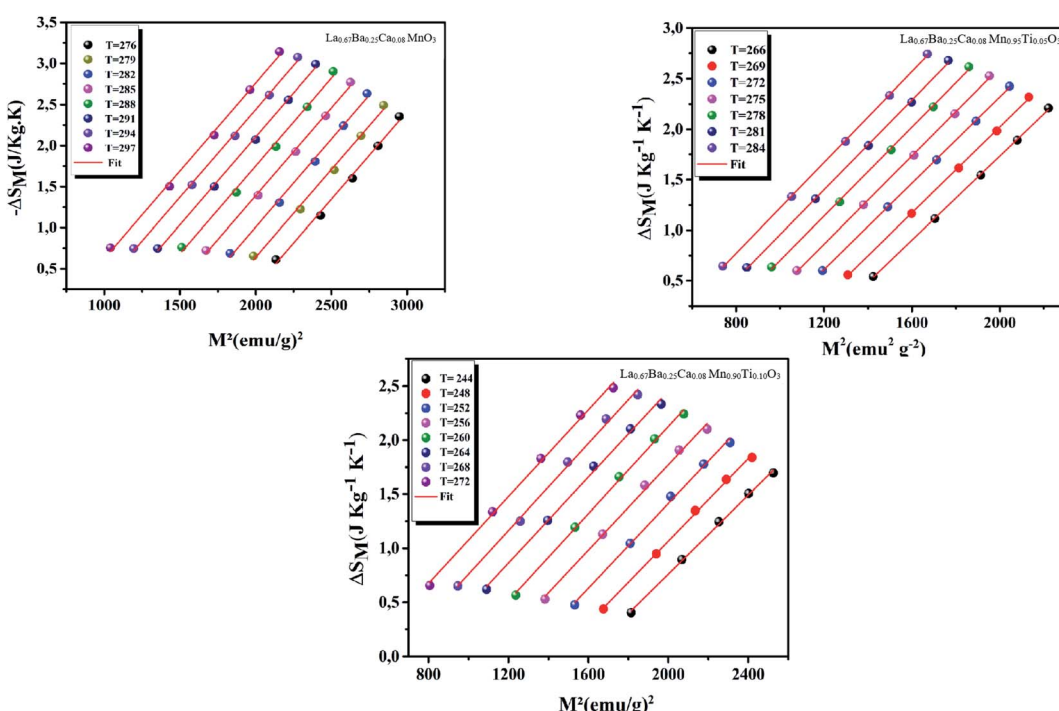


Fig. 8 Isothermal $-\Delta S_M$ vs. M^2 curves for our samples. The solid lines are linear fits to the data

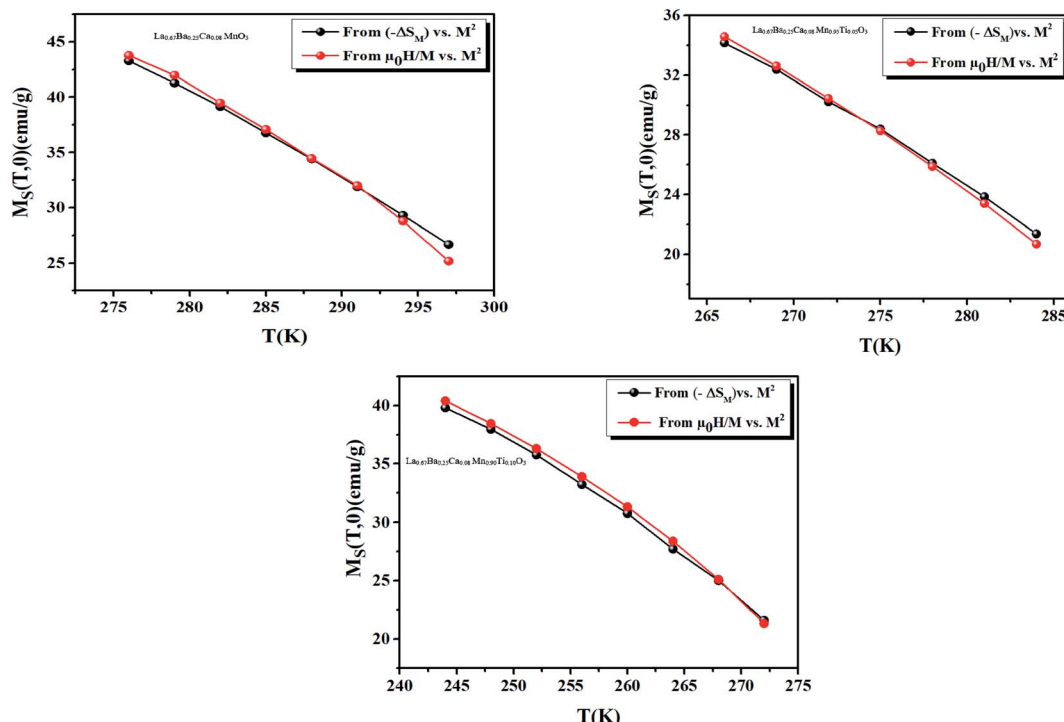


Fig. 9 Spontaneous magnetization of our samples deduced from the extrapolation of the isothermal $-\Delta S_M$ vs. M^2 curves and from the Mean-Field results.

$$S(\sigma) = -Nk_B \left[\ln(2J+1) - \ln \frac{\sinh\left(\frac{2J+1}{2J}B_J^{-1}(\sigma)\right)}{\sinh\left(\frac{1}{2J}B_J^{-1}(\sigma)\right)} + B_J^{-1}(\sigma)\sigma \right] \quad (11)$$

where N is the number of spins, k_B is the Boltzmann's constant, J is the spin value, B_J is the Brillouin's function for a given J value, and the reduced magnetization is ($\sigma = (M/gJN)\mu_B$).

For small M values, eqn (11) can be performed using a power expansion, and $-\Delta S_M$ is proportional to M^2 :

$$-\Delta S(\sigma) = \frac{3}{2} \frac{J}{J+1} Nk_B \sigma^2 + O(\sigma^4) \quad (12)$$

Moreover, below T_C , the material produces M_S . For this reason, the state $r = 0$ is never reached. If we consider only the first term of expansion of eqn (12), it is equivalent to:

$$-\Delta S(\sigma) = \frac{3}{2} \frac{J}{J+1} Nk_B (\sigma^2 + \sigma_S^2) \quad (13)$$

Eqn (13) proves that the $-\Delta S_M$ curve with respect to M^2 has a linear variation.

As seen in Fig. 8, all the curves at different temperatures (266–284 K) respect the same regularities and a clear linear variation with a nearly constant slope (0.0034), indicating that it is appropriate to analyze the current experimental results with the mean-field theory. $M_S(T)$ is then estimated from the linear adjustments of the $-\Delta S_M$ curve with respect to the M^2 curve at

different temperatures, as shown in Fig. 9. We can see that as the temperature decreases, M_S becomes larger and larger, suggesting that the compound is close to a state of rotational order at lower temperatures. The excellent agreement between the two methods confirms the validity of this process for estimating the M_S magnetization value using the mean-field analysis of $-\Delta S_M$ in our systems.

5. Conclusion

In summary, we have used magnetization measurements to study the critical phenomena at temperatures around the PM-FM phase transition in $\text{La}_{0.67}\text{Ba}_{0.25}\text{Ca}_{0.08}\text{Mn}_{(1-x)}\text{Ti}_x\text{O}_3$ ($x = 0.00, 0.05$ and 0.10) samples. The critical exponents (β, γ and δ) were obtained based on various research techniques including MAP, the KF method, and CI analysis. The estimated critical exponents confirm that the experimental values agree well with the mean-field model for our samples. The field and temperature dependent M follows the scaling theory, and all of the data fall on two distinct branches, one for $T < T_C$ and another for $T > T_C$, indicating that the critical exponents obtained in this work are accurate.

Conflicts of interest

There are no conflicts to declare.

References

- 1 E. O. Wollan and W. C. Koehler, *Phys. Rev.*, 1955, **15**, 545.

2 Y. M. Choi, M. C. Lin and M. L. Liu, *Angew. Chem. Int. Ed.*, 2007, **46**, 7214–7219.

3 J. M. Liu, Q. Huang, J. Li, C. K. Ong, Z. C. Wu, Z. G. Liu and Y. W. Du, *Phys. Rev. B: Condens. Matter Mater. Phys.*, 2000, **62**, 8976–8982.

4 O. Chmaissem, B. Dabrowski, S. Kolesnik, J. Mais, J. D. Jorgensen and S. Short, *Phys. Rev. B: Condens. Matter Mater. Phys.*, 2003, **67**, 094431.

5 A. M. Haghiri-Gosnet and J. P. Renard, *J. Phys. D: Appl. Phys.*, 2003, **36**, R127–R150.

6 E. O. Wollan and W. C. Koehler, *Phys. Rev.*, 1955, **15**, 545.

7 O. Chmaissem, B. Dabrowski, S. Kolesnik, J. Mais, J. D. Jorgensen and S. Short, *Phys. Rev. B: Condens. Matter Mater. Phys.*, 2003, **67**, 094431.

8 C. Zener, *Phys. Rev.*, 1951, **81**, 403–405.

9 Z. JiráHk, J. Hejtmánek, K. Knizek, M. Marysko, V. Sima and R. Sonntag, *J. Magn. Magn. Mater.*, 2000, **217**, 113–119.

10 M. Hazzez, N. Ihzaz, M. Boudard and M. Oumezzine, *Phys. B*, 2015, **468–469**, 39–44.

11 M. Kumaresavaji, C. T. Sousa, A. Pires, A. M. Pereira, A. M. L. Lopes and J. P. Araujo, *Appl. Phys. Lett.*, 2014, **105**, 083110.

12 M. Kačenka, O. Kaman, Z. Jirák, M. Maryško, P. Veverka, M. Veverka and S. Vratislav, *J. Solid State Chem.*, 2015, **221**, 364–372.

13 H. Baaziz, A. Tozri, E. Dhahria and E. K. Hlil, *Chem. Phys. Lett.*, 2015, **625**, 168–173.

14 D. L. Leslie-Pelecky, *Chem. Mater.*, 1996, **8**, 1770–1783.

15 T. Tajiri, H. Deguchi, S. Kohiki, M. Mito, S. Takagi, M. Mitome, Y. Murakami and A. Kohno, *J. Phys. Soc. Jpn.*, 2008, **77**, 074715.

16 Z. H. Wang, T. H. Ji, Y. Q. Wang, X. Chen, R. W. Li, J. W. Cai, J. R. Sun, B. G. Shen and C. H. Yan, *J. Appl. Phys.*, 2000, **87**, 5582–5584.

17 M. Abassi, Z. Mohamed, J. Dhahri and E. K. Hlil, *J. Alloys Compd.*, 2016, **664**, 657–663.

18 H. E. Stanley, *Rev. Mod. Phys.*, 1999, **71**, S358.

19 S. Rößler, U. K. Rößler, K. Nenkov, *et al.*, *Phys. Rev. B*, 2004, **70**, 104417.

20 A. Arrott and J. E. Noakes, *Phys. Rev. Lett.*, 1967, **19**, 786e789.

21 J. Fan, L. Ling, B. Hong, L. Zhang, L. Pi and Y. Zhang, *Phys. Rev. B: Condens. Matter Mater. Phys.*, 2010, **81**, 144426.

22 L. Xu, J. Fan, Y. Shi, Y. Zhu, K. Barner, C. Yang and D. Shi, *Europhys. Lett.*, 2015, **112**, 17005.

23 J. Engels, S. Holtmann, T. Mendes and T. Schulze, *Phys. Lett. B*, 2000, **492**, 219.

24 J. Yang, Y. Lee and Y. Li, *Phys. Rev. B: Condens. Matter Mater. Phys.*, 2007, **76**, 054442.

25 M. A. Gdaiem, A. Dhahri, J. Dhahri and E. K. Hlil, *RSC Adv.*, 2017, **7**, 10928–10938.

26 J. S. Fisher, S. K. Ma and B. G. Nickel, *Phys. Rev. Lett.*, 1972, **29**, 917–920.

27 J. S. Amaral, N. J. O. Silva and V. S. Amaral, *J. Magn. Magn. Mater.*, 2010, **322**, 1569.

28 Y. I. Spichkin and A. M. Tishin, *J. Alloys Compd.*, 2005, **403**, 38–44.

29 L. Xu, J. Fan, Y. Zhu, Y. Shi, L. Zhang, L. Pi, Y. Zhang and D. Shi, *Mater. Res. Bull.*, 2016, **73**, 187–191.

30 S. N. Kaul, *J. Magn. Magn. Mater.*, 1985, **53**, 5.

31 K. Huang, *Statistical Mechanics*, New York, 2nd ed. Wiley, 1987.

32 P. Nisha, S. Savitha Pillai, D. Azad, M. R. Varma, K. G. Suresh and H. Hahn, *Mater. Chem. Phys.*, 2012, **136**, 66.

33 M. Nasri, M. Triki, E. Dhahri and E. K. Hlil, *J. Alloys Compd.*, 2013, **546**, 84.

34 M. Oumezzine, O. Peña, S. Kallel and S. Zemni, *Solid State Sci.*, 2011, **13**, 1829.

35 A. Berger, G. Camopillo, P. Vivas, J. E. Pearson, S. D. Bader, E. Baca and P. Prieto, *J. Appl. Phys.*, 2002, **91**, 8393.

36 N. Mautis, I. Panagiotopoulos, M. Pissas and D. Niarchos, *Phys. Rev. B: Condens. Matter Mater. Phys.*, 1999, **59**, 1129.

